The Astrophysical Journal, 713:1256–1265, 2010 April 20 doi:10.1088/0004-637X/713/2/1256

NGC 2992 IN AN X-RAY HIGH STATE OBSERVED BY *XMM-NEWTON*: RESPONSE OF THE RELATIVISTIC Fe Kα LINE TO THE CONTINUUM

X. W. Shu[1,2], T. Yaqoob[2,3], K. D. Murphy[2,4], V. Braito[5], J. X. Wang[1,6], and W. Zheng[2]

[1] Center for Astrophysics, University of Science and Technology of China, Hefei, Anhui 230026, China
[2] Department of Physics and Astronomy, Johns Hopkins University, 3400 North Charles Street, Baltimore, MD 21218, USA
[3] Astrophysics Science Division, NASA/Goddard Space Flight Center, Greenbelt, MD 20771, USA
[4] Massachusetts Institute of Technology, Center for Space Research, NE80−6013, 77 Massachusetts Avenue, Cambridge, MA 02139, USA
[5] X-ray Astronomy Group, Department of Physics and Astronomy, Leicester University, Leicester, LE1 7RH, UK
[6] Key Laboratory for Research in Galaxies and Cosmology, University of Sciences and Technology of China, Chinese Academy of Sciences, Hefei, Anhui 230026, China

Received 2009 October 11; accepted 2010 March 8; published 2010 April 1

ABSTRACT

We present the analysis of an *XMM-Newton* observation of the Seyfert galaxy NGC 2992. The source was found in its highest level of X-ray activity yet detected, a factor ∼23.5 higher in the 2–10 keV flux than the historical minimum. NGC 2992 is known to exhibit X-ray flaring activity on timescales of days to weeks, and the *XMM-Newton* data provide at least a factor of ∼3 better spectral resolution in the Fe K band than any previously measured flaring X-ray state. We find that there is a broad feature in the ∼5–7 keV band that could be interpreted as a relativistic Fe Kα emission line. Its flux appears to have increased in tandem with the 2–10 keV continuum when compared to a previous *Suzaku* observation when the continuum was a factor of ∼8 lower than that during the *XMM-Newton* observation. The *XMM-Newton* data are consistent with the general picture that increased X-ray activity and corresponding changes in the Fe Kα line emission occur in the innermost regions of the putative accretion disk. This behavior contrasts with the behavior of other active galactic nuclei in which the Fe Kα line does not respond to variability in the X-ray.

Key words: galaxies: active – galaxies: Seyfert – line: profiles – X-rays: galaxies – X-rays: individual (NGC 2992)

Online-only material: color figures

1. INTRODUCTION

Relativistically broadened Fe Kα emission lines in active galactic nuclei (AGNs) and galactic black hole binaries (GBHBs) are potentially a powerful probe of accreting black hole systems. In principle, modeling the Fe Kα line profile, supplemented with assumptions about its radial and angular emissivity function in the accretion disk, can yield information on the inclination angle of the disk, its radial extent, the proximity of its inner edge to the black hole, and the angular momentum, or spin of the black hole (e.g., Dovčiak et al. 2004b; Beckwith & Done 2004; Brenneman & Reynolds 2006). While there are plenty of studies in the literature that address the *occurrence* and modeling of the time-averaged broad Fe Kα line profiles (e.g., Guainazzi et al. 2006; Nandra et al. 2007; Miller 2007, and references therein), observational data on the *variability* of the relativistic lines in AGNs are remarkably sparse (e.g., see Fabian 2006, and references therein). Variability of the line shape and intensity, especially in relation to the variability of the continuum, would provide stronger and more model-independent information on the accretion-disk and black hole parameters (in particular on the unknown radial emissivity function). It would also lay the groundwork for future reverberation mapping of the black hole metric in the strong gravity regime (e.g., Reynolds et al. 1999).

However, there are only two AGNs for which it has been possible to assess the variability of the broad Fe Kα line, and in both of those cases it is found that the line intensity does not respond to the observed X-ray continuum (MCG −6-30-15: Fabian et al. 2002; NGC 4051: Ponti et al. 2006a). Strictly speaking the NGC 4051 results refer to the reflection continuum appearing to correlate with the intrinsic continuum at small fluxes, but then remaining roughly constant as the intrinsic continuum flux increases. However, this interpretation is model dependent because the intrinsic continuum shape and flux is determined indirectly. This behavior has been interpreted in terms of the so-called light-bending model in which physical motion of the X-ray source in the strong gravity field of the black hole causes variability in the X-ray continuum for an observer "at infinity" but the illumination of the disk (and therefore the Fe Kα line flux) remains relatively unaffected. It is the variable amplification effect of light bending that causes the X-ray continuum variability—any intrinsic variability of the luminosity of the X-ray source must be suppressed or absent, otherwise the Fe Kα line intensity would once again vary. In a few other AGNs, although the variability of the Fe Kα line cannot be isolated, the overall behavior of the disk-reflection and fluorescence spectrum (of which the emission line is a part) has been interpreted as being consistent with this scenario (e.g., 1H 0707−495, Fabian et al. 2004; 1H 0419−577, Fabian et al. 2005; IRAS 13224−3809, Ponti et al. 2006b). Similar non-variability of the relativistic Fe Kα line has been observed in a GBHB (XTE J16550; Rossi et al. 2005), and this has also been interpreted in the context of the light-bending model. The origin of the physical motion of the X-ray source (relative to the black hole) and its geometry remain unspecified in the light-bending model. We note that alternative interpretations of the apparent broad Fe Kα emission lines in the above-mentioned (and other) sources in terms of absorption-only models remain viable and are still a matter of considerable debate (e.g., Miller et al. 2008, 2009; Turner et al. 2009; Turner & Miller 2009, and references therein).

The reason why so little observational data exist on the variability of the relativistic Fe Kα line, in AGN at least, is because several criteria must be met by the source at once, and such objects are not common. First, the current sensitivity of X-ray detectors requires that the source is bright enough so that the time-sliced spectra have sufficient signal-to-noise ratio. Second,

there must be a sufficient quantity of data (commensurate with the timescale of variability) in order to meaningfully test variability models. Third, the source must have a well-measured broad Fe Kα line with a large enough equivalent width (EW) so that its contrast against the continuum is high enough to constrain the line profile parameters with sufficient accuracy. Fourth, the amplitude of variability of the *continuum* should be large enough in order to be able to test whether the *line* flux varies in response to it. Although there are plenty of AGNs that satisfy one of these criteria, sources that satisfy all four are very rare. Indeed MCG −6-30-15 and NGC 4051 are the only two AGNs for which a definitive result has been reported on the non-response of the broad Fe Kα to continuum variations (as opposed to response of the broadband reflection spectrum). In this paper, we show that non-variability of the relativistic Fe Kα line in NGC 2992 in response to an increase in the X-ray continuum level is ruled out, in contrast to the known behavior of the other AGNs discussed above.

NGC 2992 is a nearby ($z = 0.00771$) Seyfert galaxy that has been observed by every major X-ray mission over the past ∼30 years, and has shown hard X-ray flux variability by more than a factor of 20 (Piccinotti et al. 1982; Turner & Pounds 1989; Turner et al. 1991; Nandra & Pounds 1994; Weaver et al. 1996; Gilli et al. 2000; Matt et al. 2003; Beckmann et al. 2007; Murphy et al. 2007; Yaqoob et al. 2007). In this paper, we describe the results of an *XMM-Newton* observation of NGC 2992 made in 2003 May. Some results from this observation from spectral fitting over a restricted bandpass (2.5–10 keV) have been presented by Brenneman & Reynolds (2009). However, Brenneman & Reynolds (2009) did not account for the heavy photon pile-up in the *XMM-Newton* CCD data, which considerably distorts the spectrum. Here we examine the data in detail, over the full *XMM-Newton* bandpass and in the context of the historical X-ray behavior of NGC 2992. During the *XMM-Newton* observation NGC 2992 was at the top end of its historical range of activity in terms of the 2–10 keV flux. We detected a strong, broad emission-line feature in the Fe K band which implies extreme variability in line flux compared to historical *Suzaku* data. This paper is organized as follows. In Section 2, we describe the *XMM-Newton* observation and data reduction. Spectral analysis of the data is described in Section 3. In Section 4, we discuss the results in detail and in Section 5 we compare the *XMM-Newton* results with those from historical data. In Section 6, we discuss some general implications of our findings and present our conclusions. A cosmology with $H_0 = 70$ km s^{-1} Mpc^{-1}, $\Lambda = 0.73$, $\Omega = 1$ is assumed throughout.

2. OBSERVATION AND DATA REDUCTION

NGC 2992 was observed by *XMM-Newton* on 2003 May 19, for a duration of about 29 ks. The EPIC pn camera and the two MOS cameras were operated in Full Window mode with a medium thick filter. We used principally the pn data, which have much higher sensitivity, using the MOS data only to check for consistency. The RGS spectral bandpass does not cover the Fe K region and the signal-to-noise ratio is poor, but we will show that our model for the pn data is consistent with the RGS spectra (see Section 3.2). The calibrated event lists were extracted from the observation data files using the EPCHAIN pipeline tasks provided by the *XMM-Newton* Science Analysis System (SAS) version 7.0.0, using the latest calibration files available at the time of the analysis (2008 February). Spectra and light curves for both the source and background were extracted using XSELECT and FTOOLS (version 6.3.2). Data were selected using different event patterns in order to investigate the effects of pile-up. Specifically, we extracted single-pixel events for both the pn and MOS, as well as single plus double-pixel events (patterns 0–4 for the pn and patterns 0–12 for the MOS). We first extracted source spectra from 40″ radius circles centered on the source position and assessed the extent of pile-up using the SAS task *epatplot*. We found that all the spectra from both *XMM-Newton* EPIC pn and MOS data at the core of the point-spread function for NGC 2992 were affected by heavy photon pile-up. Therefore, using the *epatplot* tool we compared the spectra extracted in a number of annuli with the expected distribution of energy and event grades with radius. We found that the smallest acceptable inner radius for the annular extraction region was 10″. Moreover, we found that the pn spectra made from the different pattern selections were consistent with each other. Therefore, we extracted source counts in annuli between 10″ and 40″, selecting for patterns 0–4 (pn) and 0–12 (MOS), since these event-pattern selections yielded spectra with higher signal-to-noise ratios than spectra extracted from single-pixel events.

For both pn and MOS data, the background events were extracted from source-free areas on the same CCD using two rectangular regions with a combined area 4.5 times larger than the source region. Background flares were present at the end of the observation. We adopted a count-rate filtering criterion from the full-band (∼0.3–12 keV) light curves of 0.2 ct s^{-1} (pn) and 0.1 ct s^{-1} (MOS) to remove the high particle background, which resulted in a net exposure time of ∼21.4 ks for the pn and 24.3 ks and 24.0 ks for MOS1 and MOS2, respectively. The response matrix and ancillary response file for the pn spectrum were generated using the RMFGEN and ARFGEN tools within the SAS software. We will show in Section 3.1 that the broadband 0.5–10 keV pn spectrum agrees well with the summed MOS1 and MOS2 spectra, indicating that we successfully mitigated the effect of pile-up since the severity of effect of pile-up is different for the pn and MOS data. We will further show, in Section 3.2, that the pn and RGS data are consistent with each other, indicating that any remaining effects of pile-up are negligible in the overlapping energy band.

3. SPECTRAL ANALYSIS

3.1. Preliminary Spectral Fitting

During the *XMM-Newton* observation, the source did not vary significantly in flux so we do not show the light curve. The excess variance ($\sigma^2_{\rm rms}$; see e.g., Turner et al. 1999; Markowitz & Edelson 2004) from a 0.5–10 keV pn light curve binned at 256 s (using only fully exposed bins) was found to be $\sigma^2_{\rm rms} = 0.00078 \pm 0.00018$. This value is at the lower end of the range that is typical for AGN with an intrinsic 2–10 keV luminosity similar to that of NGC 2992 (see Section 4.1). For comparison, the comparable excess variance for one of the most highly variable low-luminosity AGNs, NGC 4051, can be as high as 0.162 ± 0.0243 (Turner et al. 1999). Therefore, the spectral analysis described in the following was performed on the time-averaged spectrum.

We performed spectral fitting to the NGC 2992 *XMM-Newton* EPIC pn data in the 0.5–10 keV range using XSPEC version 11.3.2 (Arnaud 1996). The spectrum was binned uniformly to ∼40 eV per bin, and we verified that this resulted in >25 counts per bin across the full energy range, validating the use of χ^2 minimization for spectral fitting. All statistical errors given

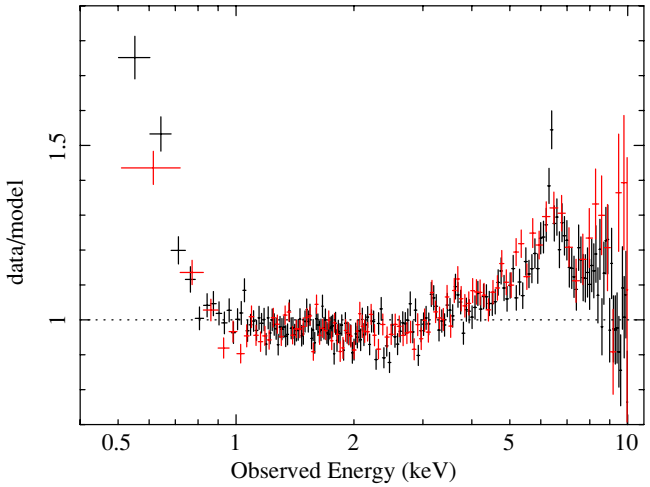

Figure 1. Ratios of the NGC 2992 *XMM-Newton* EPIC spectra to a model consisting of a simple, absorbed power-law continuum (see Section 3.1). Black and red data points correspond to the pn and summed MOS1 and MOS2 data, respectively.

(A color version of this figure is available in the online journal.)

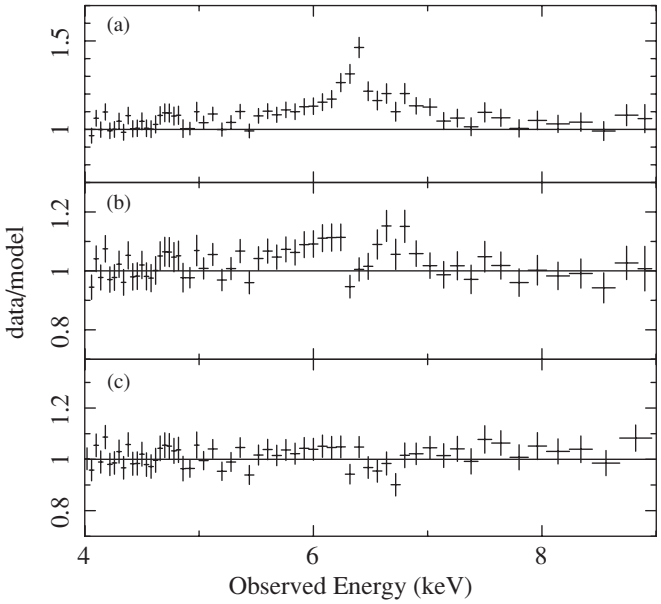

Figure 2. Data/model ratios for the NGC 2992 *XMM-Newton* pn data in the 4–9 keV band (see Sections 3.1 and 3.2 for details). (a) Data/model ratio after fitting an absorbed power-law continuum with partial covering. (b) Residuals after the narrow Kα and Kβ Fe lines have been fitted. An excess between 5.8 and 7 keV is still present. (c) Residuals after the addition of a broad Fe Kα line, using the full baseline model described in Section 3.2 (see also Table 1).

hereafter correspond to 90% confidence for one interesting parameter ($\Delta\chi^2 = 2.076$), unless stated otherwise. In all of the model fitting, the Galactic column density was fixed at $N_{\rm H} = 5.26 \times 10^{20}$ cm^{-2} (Dickey & Lockman 1990). All model parameters will be referred to in the source frame.

As an initial assessment of the form of the spectrum (with the effect of the instrumental response accounted for), in Figure 1 we show the ratio of the data to a model consisting of a simple power-law continuum with the photon index, Γ, fixed at the typical value of 1.9 (e.g., Nandra & Pounds 1994; Dadina 2008), modified by a uniform absorber. We will give spectral parameters and statistical errors below, when a full fit to the data is discussed. The spectral ratio shows that there is an excess of flux at the lowest energies and that there is still considerable curvature in the spectrum between ~4 and 8 keV. We know from previous observations of NGC 2992 that the soft flux excess is likely to be due to a combination of Thomson-thin scattering plus optically thin thermal emission in the warm extended (kpc-scale) zone that has been directly imaged by *Chandra* in NGC 2992 (Colbert et al. 2005) and in other nearby Seyfert galaxies (e.g., Morse et al. 1995). The scattered power-law continuum from this region (typically a few percent of the flux of the intrinsic power-law continuum), when combined with the intrinsic power-law emission is mathematically indistinguishable from a partial-covering model and could potentially account for at least some of the curvature in the ~4–8 keV range. Otherwise, the residuals in the ~4–8 keV range are similar to those that one would expect from a relativistically broadened Fe K line. The characteristic signature of the narrow core of the Fe K line at ~6.4 keV is also evident in the residuals. However, as explained in Sections 3.3 and 4.2, the distinction between this component and any possible relativistically broadened component may be model dependent. Figure 1 also shows the ratio of the summed MOS1 and MOS2 data to the same model, and it can be seen that the MOS data are consistent with the pn data within the statistical errors. Since the effects of pile-up are worse for the MOS than the pn, this indicates that pile-up has been mitigated.

3.2. Baseline Model

Figure 2(a) shows the data to model ratio (above 4 keV) when the absorber in the simple model above was replaced with a partial-covering model and the photon index of the power-law continuum was allowed to float (the fit was still performed in the 0.5–10 keV band). For the data/model residuals shown in Figure 2(a) the data in the 5.0–7.5 keV band, where the Fe K line emission would dominate, were omitted (and gave $\chi^2 = 234.6$ for 169 degrees of freedom). However, when the full 0.5–10 keV band data are taken into account, a poor fit was obtained, with $\chi^2 = 464.5$ for 233 degrees of freedom. Next, we added two unresolved narrow Gaussian components to model the distant-matter Fe Kα and Fe Kβ line emission. The intrinsic widths (σ_N) of the narrow Fe K lines were tied together and fixed at a value of 5 eV, much less than the pn spectral resolution (~150 eV at 6 keV). The centroid energy of the Fe Kα line ($E_{\rm N}$) and its intensity ($I_{\rm N}$) were allowed to float. The energy of the Fe Kβ line was fixed at 7.058 keV, with the line flux set equal to 13.5% of the Fe Kα as expected for neutral Fe (Kallman et al. 2004). A significant improvement in the χ^2 was obtained upon adding these two narrow lines ($\Delta\chi^2 = 107.8$ for two extra parameters). Note that when an additional broad line is included, the narrow core of the Fe Kα line becomes statistically less significant (see Section 4.2).

Figure 2(b) shows the residuals in the Fe K band after fitting the narrow Fe Kα and Kβ lines. However, it can be seen that there are still some residuals in the Fe K band indicative of additional, broader, line emission *even though some complex absorption is already included*. This excess could be associated with the line emission from the inner regions of an accretion disk. However, in principle, the residuals could alternatively be due to a continuum that is more complex than has been modeled here, and this type of degeneracy is still a matter of considerable debate (e.g., see Miller et al. 2009; Turner & Miller 2009, and references therein). For example, complex absorption and/or reflection in ionized matter could mimic relativistic Fe K line emission for data that has limited signal-to-noise ratio and spectral resolution. Although Guainazzi & Bianchi (2007) reported the detection of four

discrete absorption lines in the RGS data from the *XMM-Newton* observation reported here (C VI Lyβ, O VII Heα(r), O VIII Lyα, and O VIII Lyβ), the statistical significance of the lines was low. We attempted to model the *XMM-Newton* pn data without a broad Fe Kα relativistic line component, using a photoionized absorber instead to account for the apparent wings of the Fe Kα line. However, we found that such models (which included additional cold absorption, as well as a Compton-reflection continuum) always preferred the ionization parameter to be driven to low values (rendering the absorber only mildly unionized) and left sharp and statistically significant residuals over the narrow energy range of ∼5.5–6.5 keV. This is also evident from Figure 2: the "excess" that forms the apparent red wing of the Fe Kα line is simply too localized in energy to be explained by photoionized absorption, or for that matter, a complex continuum in general. Indeed, we found that ionized disk-reflection models (e.g., Ross & Fabian 2005) predict strong soft X-ray emission-line features that are not present in the data, and the amount of relativistic blurring required to diminish their amplitudes makes the Fe Kα line far too broad to account for the data. The case of NGC 2992 thus contrasts with the situation for MCG −6-30-15 in which the apparent red wing of the Fe Kα line is *so* broad that it is fairly easy to mimic with a complex continuum (e.g., Miller et al. 2008, 2009).

We emphasize that the importance of the *XMM-Newton* observation discussed here is that it is the *only* high-flux state observation of NGC 2992 with CCD spectral resolution. All other historical X-ray data for NGC 2992 (see Section 5) have inferior spectral resolution in the Fe K band (the source has never been observed with the *Chandra* gratings). Nevertheless, the signal-to-noise ratio is limited and does not warrant allowing black hole spin to be a free parameter when modeling the broad Fe Kα line so we used the simple model DISKLINE in XSPEC for emission from a disk around a Schwarzschild black hole (see Fabian et al. 1989). The parameters of this disk-line model are the rest-frame line energy (E_0), the inner and outer radii of the disk ($R_{\rm in}$ and $R_{\rm out}$, respectively, in units of R_g), the power-law index of the line emissivity (q, where the line emissivity is parameterized as a single power-law function, r^q), the inclination angle of the disk normal with respect to the line of sight of the observer ($\theta_{\rm obs}$), and the integrated intensity of the line, $I_{\rm disk}$. There are still too many parameters to constrain, given the degeneracies, so we fixed the inner radius at $6R_g$ (the marginally stable orbital radius for a Schwarzschild black hole), the emissivity at $q = -3$, and E_0 at 6.4 keV (corresponding to neutral Fe). For completeness, we also included an Fe Kβ disk line component with no additional free parameters, assuming the same Fe Kβ/Kα ratio as for the narrow Fe K line core. If Fe is less ionized than Fe XVII the Fe Kβ line *must* be produced.

In the final model, we also included an optically thin thermal emission component (using the APEC model in XSPEC), which we know exists from direct imaging (see Colbert et al. 2005). The relative contribution of the thermal component to the total *XMM-Newton* spectrum depends on the amplitude of the nuclear continuum because the thermal component cannot respond to variability in the nuclear continuum because of its origin in a zone that is more than 150 pc in size. As expected, since the nuclear continuum level during the *XMM-Newton* observation was at a historical high, preliminary spectral fitting showed that the relative level of the thermal emission was too low to constrain its temperature. *Suzaku* has provided the most sensitive measurement of this temperature ($kT = 0.656^{+0.088}_{-0.061}$ keV—see Yaqoob et al. 2007), so in our baseline model we fixed the temperature at the *Suzaku* value of 0.656 keV. The normalization of the thermal component was allowed to be free. However, we could only obtain upper limits on the intrinsic, absorption-corrected, luminosity of this soft thermal component of $L_{\rm apec} < 0.9 \times 10^{40}$ erg s^{-1}, which is consistent with the corresponding luminosity measured by *Suzaku*, namely, $1.18^{+0.36}_{-0.45} \times 10^{40}$ erg s^{-1} (Yaqoob et al. 2007).

In our baseline model, we also included a Compton-reflection component using the model PEXRAV in XSPEC (see Magdziarz & Zdziarski 1995). Although the *XMM-Newton* data do not have a sufficiently wide bandpass to constrain any possible reflection component well, it can potentially affect deduced Fe K line parameters. The reflection continuum affects only the 6–10 keV band, so the results must be interpreted with caution. The only parameter we allowed to be free in the reflection model was the so-called reflection fraction, R, which is the normalization of the reflection continuum relative to the case of a steady state, centrally illuminated, neutral disk subtending a solid angle of 2π at the X-ray source. We note that our modeling of a possible reflection continuum should be interpreted as an empirical parameterization only because the disk geometry may not be appropriate for all of the Compton reflection.

In summary, our baseline model consists of 12 free parameters: the normalization of the power-law continuum, its slope (Γ), the intrinsic absorbing column density (N_H), the covering fraction (f_c), $E_{\rm N}$, σ_N, $I_{\rm N}$, the reflection fraction (R), $\theta_{\rm obs}$, $R_{\rm out}$, $I_{\rm disk}$, and the normalization of the optically thin thermal continuum component. We interpret the partial-covering model in terms of a fully covered X-ray source plus a fraction (f_s) of the intrinsic continuum scattered into the line of sight by a warm, optically thin scattering zone, so that $f_s = (1 - f_c)/f_c$. In this scenario, if the scattering zone has a Thomson depth $\tau_{\rm es}$, and if the portion of the scattering zone that is visible to the observer subtends a solid angle Ω at the X-ray source, $f_s = \tau_{\rm es}(\Omega/4\pi)$. This baseline model gives an excellent fit to the *XMM-Newton* data ($\chi^2 = 282.5$ for 225 degrees of freedom). The best-fitting parameters and their statistical errors are shown in Table 1 and will be discussed in detail in Section 4.

Figure 3 shows the best-fitting baseline model spectrum and the data/model residuals. The data/model residuals for the same model are also shown in Figure 2(c) for just the 4–9 keV band in order to display the Fe K region more clearly. It can be seen that there are still some line-like residuals in the ∼6.5–7.5 keV band. These are likely to be due to Fe XXVI Lyα and Ni Kα emission lines which have rest-frame energies of 6.966 keV (Pike et al. 1996) and 7.472 keV (Bearden 1967), respectively. However, these features are not statistically significant: when modeled with narrow Gaussian components with centroid energies fixed at the above values, and with widths fixed at 5 eV, the residuals vanish but the overall value of χ^2 is reduced by only 8.6 for the addition of two free parameters. We obtained EW $= 24^{+15}_{-16}$ eV for the Fe XXVI Lyα line and for the Ni Kα line we obtained only an upper limit of 34 eV for the EW. Thereafter, we did not include the Fe XXVI Lyα and Ni Kα lines in our baseline model.

Figure 4 shows the unfolded pn spectrum and best-fitting continuum model. Overlaid on this are the unfolded RGS1 and RGS2 data (the Fe K emission-line components have been removed to prevent the formation of artificially narrow spectral features in the unfolded pn spectrum). No adjustment was made to any relative normalizations for overlaying the RGS data, and the excellent agreement between the RGS and pn data shows that the effects of pile-up in the pn data have been successfully mitigated in the overlapping energy band. It can also be seen

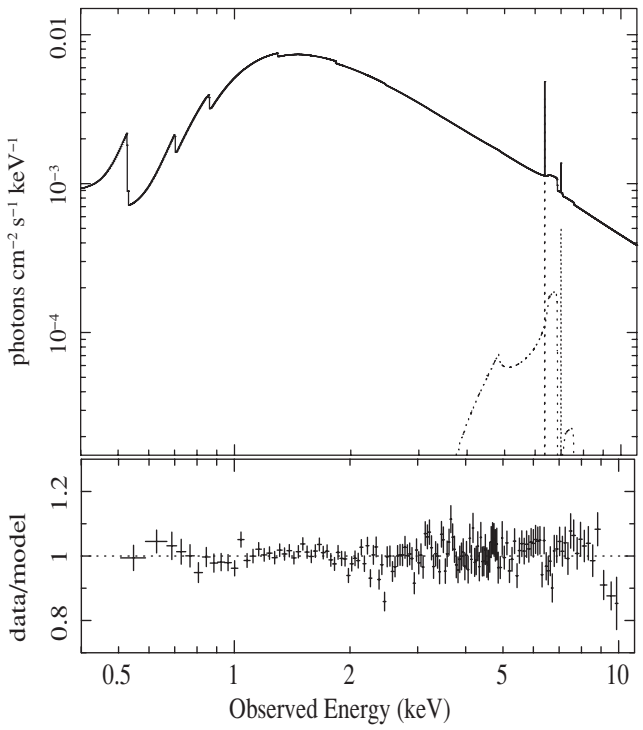

Figure 3. Best-fitting baseline model to the NGC 2992 *XMM-Newton* pn data (top panel) and the corresponding data/model ratio (bottom panel; see Section 3.2 and Table 1 for details).

Table 1
Spectral Fitting Results for NGC 2992 *XMM-Newton* Data

Parameter	Value
χ^2/degrees of freedom	282.5/225
$L_{\rm APEC}$ (10^{40} erg s^{-1})	< 0.9
Γ	$1.83^{+0.06}_{-0.04}$
N_H (10^{21} cm^{-2})	$6.45^{+0.25}_{-0.17}$
f_s (scattered fraction)	$0.013^{+0.002}_{-0.002}$
$\theta_{\rm obs}$ (degrees)	$38.0^{+2.7}_{-6.3}$
Reflection fraction, R	$0.40(< 1.16)$
Outer radius of disk, $R_{\rm out}$	$14.7^{+71.4}_{-4.5}$
$I_{\rm disk}$ [Fe Kα] (10^{-5} photons cm^{-2} s^{-1})	$24.1^{+6.3}_{-6.3}$
EW$_{\rm disk}$ [Fe Kα] (eV)	255^{+67}_{-67}
E_N [Fe Kα] (keV)	$6.403^{+0.025}_{-0.027}$
σ_N (keV)	< 0.083
FWHM (km s^{-1})	$< 9\,155$
$I_{\rm N}$ [Fe Kα] (10^{-5} photons cm^{-2} s^{-1})	$5.7^{+2.6}_{-3.1}$
EW$_{\rm N}$ [Fe Kα] (eV)	49^{+22}_{-27}
$F_{0.5-2\ \rm keV}$ (10^{-11} erg cm^{-2} s^{-1})[a]	1.8
$F_{2-10\ \rm keV}$ (10^{-11} erg cm^{-2} s^{-1})[a]	9.5
$L_{0.5-2\ \rm keV}$ (10^{43} erg s^{-1})[b]	0.84
$L_{2-10\ \rm keV}$ (10^{43} erg s^{-1})[b]	1.3

Notes. Statistical errors and upper limits correspond to 90% confidence for one interesting parameter ($\Delta\chi^2 = 2.706$) and were derived with 12 parameters free. See Section 3.2 for details of the model. Note that the constraints on $R_{\rm out}$ correspond to a local minimum only and should be interpreted with caution (see the text for details). All parameters (except continuum fluxes) refer to the rest frame of NGC 2992.

[a] Observed-frame fluxes, *not* corrected for Galactic and intrinsic absorption.

[b] Intrinsic, rest-frame luminosities, corrected for all absorption components.

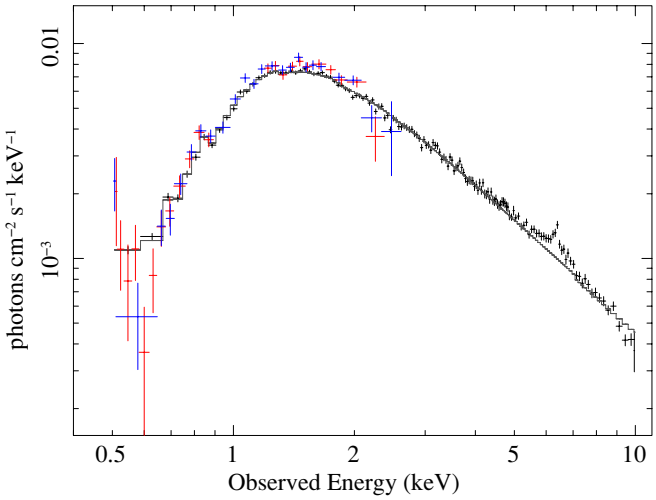

Figure 4. Unfolded *XMM-Newton* pn data for NGC 2992 (using the best-fitting baseline model described in Section 3.2, with the emission-line features removed in order to avoid artificial narrow features in the unfolded spectrum). Overlaid are the RGS1 (red) and RGS2 (blue) data, with no relative normalization adjustments. This shows that effects of pile-up in the pn spectrum have been successfully mitigated in the overlapping bandpass.

(A color version of this figure is available in the online journal.)

that the signal-to-noise ratio of the RGS data is unfortunately very poor. Since the count rate for the pn spectrum is so much higher than the count rates for the RGS spectra, spectral fits would be overwhelmingly dominated by the pn data. For these reasons we did not consider the RGS data further.

3.3. Broad versus Narrow Fe K Line

Here, we give the results of investigating the extent to which the broad Fe K disk-line component and the narrow, distant-matter Fe K line (e.g., see Yaqoob & Padmanabhan 2004) may be decoupled from modeling of the *XMM-Newton* data. Using the best-fitting baseline model (Section 3.2 and Table 1), we constructed two-parameter joint confidence contours of the disk-line intensity ($I_{\rm disk}$) versus the narrow-line intensity (I_N), while allowing the other 10 free parameters of the model to remain free. Figure 5 shows the resulting 68%, 90%, and 99% confidence contours. For comparison, the corresponding confidence contours obtained by Yaqoob et al. (2007) from *Suzaku* data are shown in Figure 5. So far, *Suzaku* has provided the best measurement of the distant-matter Fe Kα line in NGC 2992 because the continuum happened to be low and because of the high throughput and sensitivity of *Suzaku*. It can be seen that at 99% confidence the narrow Fe Kα line intensity from the *XMM-Newton* data could formally be zero, but values of up to a factor of $\sim$4 greater than the *Suzaku* value of $\sim 2.5 \times 10^{-5}$ photons cm^{-2} s^{-1} (Yaqoob et al. 2007) are not ruled out. In the *XMM-Newton* data, the narrow Fe Kα line is marginal because it is weak against the much higher continuum compared with that in the *Suzaku* data. On the other hand, the broad Fe Kα line component is strong in the *XMM-Newton* data, and the intensity is required to be non-zero at a high level of significance in the context of the baseline model fitted here. Indeed, the intensity of the broad line appears to be an order of magnitude larger than that measured by *Suzaku* (Yaqoob et al. 2007), and Figure 5 shows that the 99% confidence contours for the *XMM-Newton* and *Suzaku* data are mutually exclusive, indicating strong variability of the broad Fe K line component.

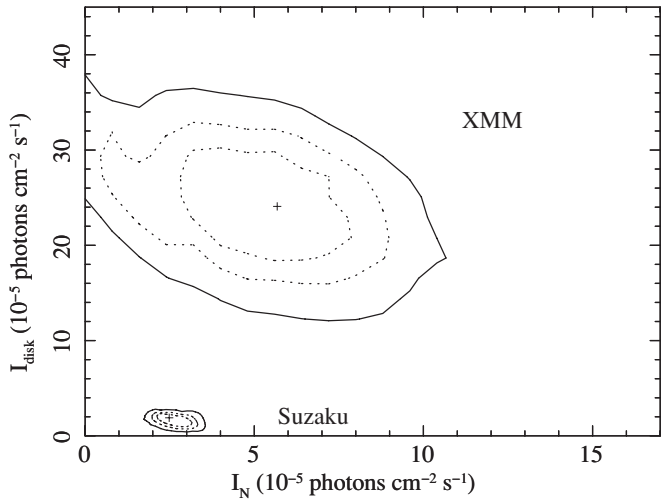

Figure 5. 68%, 90%, and 99% confidence contours of the broad Fe Kα line intensity, ($I_{\rm disk}$), vs. the intensity of the narrow Fe Kα line, ($I_{\rm N}$), for the NGC 2992 *XMM-Newton* data (see Section 3.1 for details). Also shown for comparison are the corresponding confidence contours for the *Suzaku* NGC 2992 data reported in Yaqoob et al. (2007).

4. DETAILED RESULTS

We now discuss in detail the results that were obtained from fitting the baseline model (Section 3.2) to the *XMM-Newton* pn data for NGC 2992 (see Table 1).

4.1. Continuum

We obtained $\Gamma = 1.83^{+0.06}_{-0.04}$ for the power-law photon index of the intrinsic continuum and a column density of $6.45^{+0.25}_{-0.17} \times 10^{21}$ cm^{-2} for the line-of-sight X-ray obscuration (see Table 1). A comparison with historical data is given in Section 5. Table 1 shows that we measured (1.3% $\pm$ 0.2%) for the continuum scattered into the line of sight, as a percentage of the direct line-of-sight continuum before absorption. *Suzaku* data provided one of the best measurements of the scattered continuum (Yaqoob et al. 2007), again because of *Suzaku*'s sensitivity and because of the low level of the nuclear continuum at the time of the *Suzaku* observations. The corresponding scattered percentage from *Suzaku* was larger (7.3%$\pm$2.1%) than that measured from the *XMM-Newton* data because the scattered continuum originates in an extended zone larger than 150 pc (Colbert et al. 2005) and the direct continuum during the *XMM-Newton* observation was at least a factor of 8 greater than that during the *Suzaku* observations. Clearly, some variability in the absolute level of the scattered continuum is indicated (a factor of $\sim$1.5), but it cannot respond to short-term variations in the direct continuum and its absolute luminosity must correspond to an appropriate historically averaged level of the intrinsic X-ray continuum. In Yaqoob et al. (2007), we deduced a value of the Thomson depth for the warm scattering zone of $\tau_{\rm es} \sim 0.1$, and the *XMM-Newton* data are consistent with that, given that the intrinsic continuum during the *XMM-Newton* observation is likely to be a factor of $\sim$5–6 higher than the continuum level averaged over more than a year (see Murphy et al. 2007).

4.2. Fe K Emission Lines

In Section 3.3 and Figure 5, we showed that the *XMM-Newton* data do not allow deconvolution of the broad, relativistic Fe K line component from the narrow-line core. This is because the continuum during the *XMM-Newton* observation was high, but the narrow line originates from a larger region, at least the size of the BLR, so cannot respond to short-term continuum changes. Therefore, the narrow-line EW was low, and the line parameters were more difficult to measure than those from the narrow line in the 2005 *Suzaku* data in which the continuum was a factor of $\sim$8 lower than that found in the *XMM-Newton* observation. The *Suzaku* measurements of the Fe Kα line core parameters are the best to date because of the sensitivity of *Suzaku* and because the EW of the Fe Kα line core was particularly large during the *Suzaku* observations (see Yaqoob et al. 2007). Thus, both the EW and intensity of the narrow Fe K line were poorly constrained by the *XMM-Newton* data, having values 49^{+22}_{-27} eV and $5.7^{+2.6}_{-3.1} \times 10^{-5}$ photons cm^{-2} s^{-1}, respectively (see Table 1). As indicated by the statistical errors, given the degeneracies, the narrow Fe K line was not in fact significantly detected in the *XMM-Newton* data. However, the *XMM-Newton* data are consistent with the narrow Fe K line being present with the same absolute intensity as in the *Suzaku* data (see Section 3.1 and Figure 5). The upper limit on the width of the narrow Fe K line obtained from the *XMM-Newton* data (FWHM < 9155 km s^{-1}) was also looser than the corresponding *Suzaku* constraint (FWHM < 4850 km s^{-1}). See Yaqoob et al. (2007) for a discussion of the associated constraints on the location of the matter responsible for the Fe K line core.

On the other hand, the *XMM-Newton* data provide very strong constraints on a possible broad, relativistic Fe Kα emission-line component because that component appears to have increased in absolute flux in tandem with the intrinsic continuum level, compared to the *Suzaku* data. From simple modeling of the *XMM-Newton* data we obtained a broad Fe Kα line flux of $I_{\rm disk} = 24.1^{+6.3}_{-6.3} \times 10^{-5}$ photons cm^{-2} s^{-1} (Table 1), compared to the *Suzaku* value of $1.9^{+0.5}_{-1.0} \times 10^{-5}$ photons cm^{-2} s^{-1} (Yaqoob et al. 2007). The *Suzaku* data gave the most sensitive and highest spectral-resolution measurements of the broad Fe Kα component when the X-ray continuum was in a low state. Thus, an order of magnitude increase in the continuum level appears to have been accompanied by a similar factor increase in the flux of the broad Fe Kα line. Our measurement of the broad Fe Kα line flux is consistent, within the statistical errors, with Brenneman & Reynolds (2009) but they did not account for the severe pile-up in the data (and they also used a different model and a narrower bandpass).

Next, we investigated the sensitivity of the broad Fe Kα line flux in the *XMM-Newton* data to the Compton-reflection continuum. Table 1 shows that we obtained only an upper limit on the best-fitting value for the Compton-reflection continuum relative normalization of $R < 1.16$, but the *XMM-Newton* bandpass can only cover a small portion of the Compton-reflection continuum. For the *XMM-Newton* data, we constructed joint confidence contours of the broad Fe Kα line intensity, $I_{\rm disk}$, versus R. We found that at 99% confidence the lower limit on $I_{\rm disk}$ was at least non-zero over the range $0 \leqslant R \leqslant 3$ and was never less than 10^{-4} photons cm^{-2} s^{-1}. Thus, we conclude that the broad Fe Kα line intensity is not sensitive to the fitted normalization of the Compton-reflection continuum.

From our simple model we found that the outer disk radius ($R_{\rm out}$) for the broad Fe Kα line emission is sensitive to the radial emissivity parameter, q. For $q = -3$, as adopted here, we could only obtain loose constrains of $R_{\rm out}$ of $14.7^{+71.4}_{-4.5} R_g$ (statistical errors correspond to 90% confidence for one parameter, or $\Delta\chi^2 = 2.706$). We note, however, that this solution for $R_{\rm out}$ is a local minimum only, and the value of $\Delta\chi^2$ drops below 2.7 more than once outside the above range. At $R_{\rm out} = 6.1 R_g$,

$\Delta\chi^2 = 2.82$, and at $R_{\rm out} = 1000R_g$, $\Delta\chi^2 = 1.89$. In other words, $R_{\rm out}$ is very poorly constrained. We found that a steeper radial emissivity law tends to favor larger upper limits on $R_{\rm out}$ and a flatter emissivity law gives smaller preferred values on the upper bound on the outer radius. For example, with $q = -2$, $R_{\rm out} = 14.0^{+7.4}_{-3.7} R_g$ (again the errors correspond to 90% confidence for one parameter, but the minimum in χ^2 is more robust, giving a lower limit on $R_{\rm out}$ as well as an upper limit). We found fairly tight constraints on the disk inclination angle, obtaining $\theta_{\rm obs} = 38.0^{+2.7}_{-6.3}$ deg (Table 1). This is consistent with the lower limit obtained from the broad Fe Kα line component in the *Suzaku* data ($\theta_{\rm obs} > 31^\circ$—see Yaqoob et al. 2007).

5. COMPARISON WITH OTHER HISTORICAL DATA

In Section 5.1, we discuss the *XMM-Newton* observation of NGC 2992 in the general context of the historical broadband spectra, flux, and variability. In Section 5.2, we discuss how the detailed X-ray spectroscopy of the Fe K band in NGC 2992 based on the *XMM-Newton* data compares with historical data.

5.1. X-ray Variability History of NGC 2992

Murphy et al. (2007) showed a historical light curve of NGC 2992 spanning ∼30 years, going back to *HEAO*-1. The 2–10 keV flux varied by a factor of over 20, with an *ASCA* observation in 1994 (Weaver et al. 1996) still holding the record for the lowest 2–10 keV observed flux ($\sim 4 \times 10^{-12}$ erg cm^{-2} s^{-1}). The *ASCA* data revealed a very prominent, narrow Fe Kα emission line, with an EW ∼ 500 eV. The narrow-line intensity had not responded to the declining continuum, indicating that this particular line component likely arose in matter far from the supermassive black hole (possibly in the putative obscuring torus). Later, two *BeppoSAX* observations in the period 1997–1998 (Gilli et al. 2000) yielded data corresponding to continuum levels that were different by an order of magnitude to each other, revealing Fe K line emission that was more complicated than previous data had indicated. There was evidence for possible contributions from both the accretion disk and distant matter, as well as line components from highly ionized Fe. More recently, a 1 year monitoring campaign of NGC 2992 with *RXTE* beginning in 2005 revealed that strong continuum flux variations by a factor of up to ∼11 (from $\sim(0.8–9) \times 10^{-11}$ erg cm^{-2} s^{-1} in the 2–10 keV band) actually occur frequently, on timescales of days to weeks (Murphy et al. 2007). Additionally, during high-flux periods the spectrum was dominated by a highly redshifted and broadened Fe Kα emission line. Murphy et al. (2007) interpreted this redshifted and broadened Fe Kα line in the high continuum state in terms of the temporary enhancement of line emission from the inner region of the accretion disk ($<100R_g$), where strong gravitational and Doppler effects are important. Still, there were considerable degeneracies in the *BeppoSAX* and *RXTE* data. Meanwhile, *Suzaku* observations of NGC 2992 at the end of 2005 caught the source in a relatively low state with a 2–10 keV flux of 1.1×10^{-11} erg cm^{-2} s^{-1} (Yaqoob et al. 2007). In particular, the complex Fe Kα line emission profile, consisting of a low-level, "persistent" accretion-disk component and a distant-matter component, was observed and could be decoupled at a confidence level greater than 3σ. Hard X-ray data taken by *INTEGRAL* (in 2005 May) and *Swift* (in 2005–2006) showed that the X-ray continuum extends to at least ∼200 keV, but the data were not sensitive enough to perform further detailed spectroscopy of the Fe K line complex (Beckmann et al. 2007). The *XMM-Newton* observation reported in this paper represents the highest 2–10 keV flux state of NGC 2992 ever observed.

5.2. Historical X-ray Spectral Results

We now investigate whether historical X-ray spectra for NGC 2992 can be understood in terms of the baseline model that has been used to fit the *XMM-Newton* data. Only *Suzaku* data (Yaqoob et al. 2007) have spectral resolution and signal-to-noise ratio that are comparable to the *XMM-Newton* data, and comparisons between the two data sets have been given throughout this paper. The two data sets are consistent with both narrow and broad Fe Kα lines being present, but in the *XMM-Newton* data (high-flux state) the broad line dominated, and in the *Suzaku* data (low-flux state), the narrow line dominated. Unfortunately, the spectral resolution and/or signal-to-noise ratio of most of the other historical data are not sufficient to perform meaningful fits with a dual (broad plus narrow) Fe Kα line model. Thus, we performed such an analysis only on the historical 1994 *ASCA* spectrum and the 1997 and 1998 *BeppoSAX* spectra. It is difficult to compare our fits to the *XMM-Newton* data with published results in the literature for the *ASCA* and *BeppoSAX* data because different models have been used to fit the data. We therefore used the same baseline model as that used to fit the *XMM-Newton* data (Section 3.2) but fixed several parameters due to the poorer signal-to-noise ratio (and in the case of the *BeppoSAX* data poorer spectral resolution as well). The inclination angle ($\theta_{\rm obs}$) of the accretion disk and the outer radius of emission on the disk ($R_{\rm out}$) were fixed at the respective best-fitting values from the fit to the *XMM-Newton* data (Table 2). The *ASCA* data were fitted in the range 0.5–10 keV and the *BeppoSAX* data were fitted in the range 1–100 keV using both the MECS and PDS instruments (see Gilli et al. 2000). Neither the *ASCA* nor the *BeppoSAX* data could constrain the luminosity of the soft thermal emission component (Section 3.2), so it was not included in the fits, but it was possible to obtain an upper limit on its luminosity for the *ASCA* data. All of the spectral fitting results for the *ASCA* and *BeppoSAX* data are shown in Table 2.

Within the statistical errors, the power-law slope appears to be consistent among the different data sets, including the *XMM-Newton* data. However, variability in the slope cannot be ruled out. On the other hand, the column density measured from the *XMM-Newton* data is formally inconsistent with that measured from the two *BeppoSAX* observations. However, the *BeppoSAX* data only extend down to 1 keV and the spectral resolution is poorer than the *XMM-Newton* data so any variability in the column density must be interpreted with caution.

As might be expected, the broad Fe Kα line intensity could not be constrained by the *ASCA* data and the low-state *BeppoSAX* data, and only upper limits could be obtained. However, for the high-state (1998) *BeppoSAX* data we measured the broad-line intensity to be $14.7^{+9.1}_{-9.8} \times 10^{-5}$ photons cm^{-2} s^{-1}. This is lower than the corresponding intensity measured during the *XMM-Newton* observation and higher than that measured during the *Suzaku* observation. However, the 99% confidence, two-parameter broad-line intensity contours from both *XMM-Newton* and *Suzaku* overlap the *BeppoSAX* measurement (see Figure 5). Nevertheless, the collective data are not inconsistent with the broad-line flux responding to variability in the continuum flux (see Tables 1 and 2 for continuum fluxes).

We confirmed the large EW of the narrow Fe Kα line at ∼6.4 keV during the *ASCA* observation (see Table 2), when the X-ray spectrum was dominated by a scattered continuum

Table 2
Spectral Fitting Results for Historical NGC 2992 Data

Parameter	*ASCA* (1994)	*BeppoSAX* (1997–SAX1)	*BeppoSAX* (1998–SAX2)
χ^2/degrees of freedom	99.2/136	189.9/204	253.9/248
$L_{\rm APEC}$ (10^{40} erg s^{-1})	< 3.1	...	...
Γ	$1.50^{+0.72}_{-0.32}$	$2.08^{+0.34}_{-0.31}$	$1.79^{+0.07}_{-0.06}$
N_H (10^{21} cm^{-2})	$9.4^{+5.3}_{-7.1}$	$33.5^{+15.8}_{-17.1}$	$12.4^{+8.0}_{-3.8}$
$f_{\rm s}$ (scattered fraction)	$1.0^{+3.9}_{-0.7}$	$0.35^{+0.32}_{-0.23}$	$0.18^{+0.38}_{-0.18}$
Reflection fraction, R	...	$2.6^{+4.8}_{-2.1}$	$0.1^{+0.2}_{-0.1}$
$I_{\rm disk}$ [Fe Kα] (10^{-5} photons cm^{-2} s^{-1})	< 5.6	< 1.8	$14.7^{+9.1}_{-9.8}$
EW$_{\rm disk}$ [Fe Kα] (eV)	< 1190	< 150	188^{+115}_{-125}
E_N [Fe Kα] (keV)	$6.41^{+0.05}_{-0.05}$	6.4 (f)	6.4 (f)
$I_{\rm N}$ [Fe Kα] (10^{-5} photons cm^{-2} s^{-1})	$2.6^{+1.4}_{-1.3}$	< 2.1	$2.8^{+3.6}_{-2.8}$
EW$_{\rm N}$ [Fe Kα] (eV)	506^{+272}_{-253}	< 184	32^{+39}_{-32}
Ionized line, E	...	$6.60^{+0.12}_{-0.06}$	$7.08^{+0.31}_{-0.39}$
Ionized line, I	...	$3.4^{+0.7}_{-0.8}$	$2.5^{+2.3}_{-2.1}$
Ionized line, EW	...	494^{+102}_{-116}	35^{+32}_{-29}
$F_{0.5-2\ \rm keV}$ (10^{-11} erg cm^{-2} s^{-1})[a]	0.086	...	...
$F_{2-10\ \rm keV}$ (10^{-11} erg cm^{-2} s^{-1})[a]	0.44	0.59	7.4
$L_{0.5-2\ \rm keV}$ (10^{43} erg s^{-1})[b]	0.022	...	...
$L_{2-10\ \rm keV}$ (10^{43} erg s^{-1})[b]	0.060	0.092	1.1

Notes. Note that results of fits to historical *Suzaku* data using a similar model can be found in Yaqoob et al. (2007). Statistical errors and upper limits correspond to 90% confidence for one interesting parameter ($\Delta\chi^2 = 2.706$) and were derived with eight parameters free. All parameters (except continuum fluxes) refer to the rest frame of NGC 2992. Some of the disk and distant-matter Fe Kα emission-line parameters were frozen—see Section 5 for details of the model. Frozen parameters are indicated by "(f)".

[a] Observed-frame fluxes, *not* corrected for Galactic and intrinsic absorption.

[b] Intrinsic, rest-frame luminosities, corrected for all absorption components.

and the narrow Fe Kα line, neither of which had responded to the dramatic decline in the continuum flux compared to earlier epochs (see Murphy et al. 2007). However, the behavior of the narrow Fe Kα line during the *BeppoSAX* observations is puzzling. In the low-state (1997) *BeppoSAX* observation the narrow line at 6.4 keV was not detected (but the upper limit on its flux, as shown in Table 2, is consistent with historical data). However, there is instead a statistically significant ($\Delta\chi^2 = 30.2$ for the addition of two free parameters) narrow emission line at $6.60^{+0.12}_{-0.06}$ keV (see Table 2 for parameters). During the high-state (1998) *BeppoSAX* observation the narrow line at 6.4 keV was again marginally detected ($\Delta\chi^2 = 1.7$), but its flux is formally consistent with that during the *ASCA* observation (for 90% confidence, one parameter). Moreover, in the 1998 *BeppoSAX* data there are residuals that can be modeled by an additional ionized Fe emission line at $7.08^{+0.31}_{-0.39}$ keV, but the statistical significance is low ($\Delta\chi^2 = 3.5$). All of these unusual features have already been noted in earlier analyses of the 1997 and 1998 *BeppoSAX* data (Gilli et al. 2000).

5.3. Variation of the Reflection Spectrum

We note that an increase in the flux of the Fe Kα line, as observed during the *XMM-Newton* observation, compared to historical data, should be accompanied by a corresponding increase in the magnitude of the associated continuum reflection. This is because the relativistic component of the Fe Kα line and the reflection continuum both originate from reprocessing the same intrinsic continuum at the same physical locations so the flux of the line relative to the reflection continuum should not itself vary as the intrinsic continuum varies. We have applied the reflection model KYL1CR, which is publicly available for the XSPEC package, to the *XMM-Newton* and *Suzaku* data. The model calculates the reflection continuum and the associated Fe Kα and Fe Kβ emission lines self-consistently for a neutral disk, including relativistic blurring applied to continuum and emission lines. Full details of the model and its parameters can be found in Dovčiak et al. (2004a). The model is only valid above 2 keV so we fitted both data sets in the 2–10 keV band. The purpose here is to simply assess whether these two data sets, representing low (*Suzaku*) and high (*XMM-Newton*) continuum states, are at least consistent with the entire reflection spectrum (continuum plus broad emission lines) following the order-of-magnitude change in continuum flux between the *Suzaku* and *XMM-Newton* observations. Since the fits were performed only above 2 keV, we fixed the absorbing column density, N_H, and the scattering fraction, f_s, at the best-fitting values for *XMM-Newton* (Table 1) and *Suzaku* (Yaqoob et al. 2007). The soft thermal emission component was omitted as it has no impact on the fitted energy band. The inner and outer radii of the disk were fixed at $6R_g$ and $1000R_g$, and the disk radial emissivity index, q, was fixed at -3. The black hole spin was fixed at a value of zero. The KYL1CR model includes the Fe Kβ as well as the Fe Kα emission line. Narrow Gaussian emission lines to model the distant-matter Fe Kα and Fe Kβ emission lines were still included but the centroid energies and intrinsic line widths were fixed at the best-fitting values from the appropriate empirical fits in Table 1 and Yaqoob et al. (2007). Our conclusions with respect

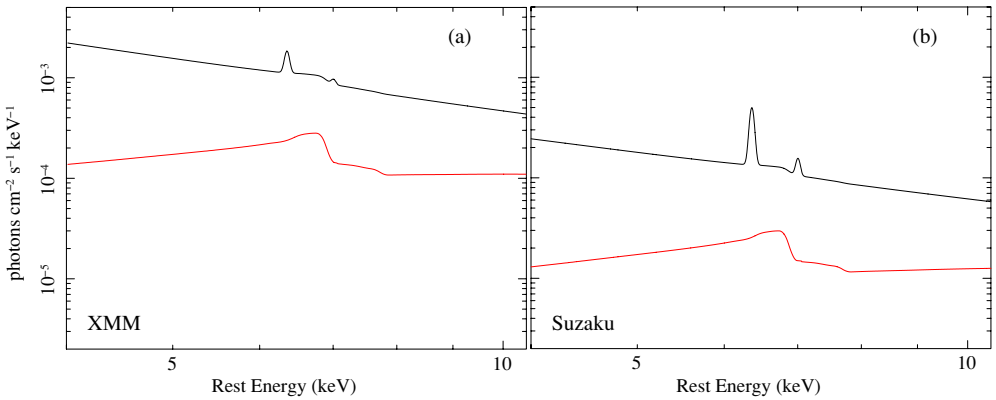

Figure 6. Best-fitting KYL1CR models to (a) the *XMM-Newton* data and (b) the *Suzaku* data. The black spectra correspond to the sum of the intrinsic power-law continuum plus the reflection continuum and broad and narrow Fe Kα and Fe Kβ emission lines, and the red spectra correspond to the reflection components only (i.e., reflected continuum disk emission lines after relativistic blurring). The 4–10 keV band is shown in order to exhibit greater details in the complex Fe K region of the spectra.

(A color version of this figure is available in the online journal.)

Table 3
Spectral Fitting Results for the KYL1CR Model

Parameter	*XMM-Newton*	*Suzaku*
χ^2/degrees of freedom	245.8/193	240.3/267
Reduced $\chi^{2\,a}$	1.27	0.90
Γ	$1.99^{+0.13}_{-0.05}$	$1.75^{+0.10}_{-0.10}$
$\theta_{\rm obs}$ (degrees)	$40.7^{+3.3}_{-4.6}$	$39.8^{+4.1}_{-4.7}$
KYL1CR normalization[b]	$1.18^{+0.15}_{-0.16} \times 10^{-4}$	$1.09^{+0.36}_{-0.48} \times 10^{-5}$
$I_{\rm N}$ [Fe Kα] (10^{-5} photons cm^{-2} s^{-1})	$6.1^{+1.6}_{-1.5}$	$3.1^{+0.3}_{-0.3}$
EW$_{\rm N}$ [Fe Kα] (eV)	53^{+14}_{-13}	218^{+21}_{-21}
$F_{2-10\ \rm keV}$ (10^{-11} erg cm^{-2} s^{-1})[c]	9.5	1.1
$L_{2-10\ \rm keV}$ (10^{43} erg s^{-1})[d]	1.3	0.16

Notes. Results of spectral fitting with the relativistic disk model KYL1CR (see Section 5.3 for details). Statistical errors and upper limits correspond to 90% confidence for one interesting parameter ($\Delta\chi^2 = 2.706$) and were derived with five parameters free. All parameters (except continuum fluxes) refer to the rest frame of NGC 2992.

[a] For comparison, the reduced χ^2 values for the fits with PEXRAV were 1.28 and 0.89 for the *XMM-Newton* (Table 1) and *Suzaku* (Yaqoob et al. 2007) data, respectively.

[b] The definition of the normalization of the reflection spectrum is peculiar to the KYL1CR model and is defined as the monochromatic flux at 3 keV in units of photons cm^{-2} s^{-1} keV^{-1} (see Dovčiak et al. 2004a).

[c] Observed-frame fluxes, *not* corrected for Galactic and intrinsic absorption.

[d] Intrinsic, rest-frame luminosities, corrected for all absorption components.

to variability of the disk-reflection features are not sensitive to these parameters. This left a total of five free parameters for the error analysis, namely, the intrinsic power-law normalization, photon index (Γ), the reflection spectrum normalization, the disk inclination angle, and the flux of the narrow Fe Kα line from distant matter. Note that the definition of the normalization of the reflection spectrum here is peculiar to the KYL1CR model, being the flux of the reflection spectrum at 3 keV in units of photons cm^{-2} s^{-1} keV^{-1} (see Dovčiak et al. 2004a for details).

The results of the KYL1CR fits are shown in Table 3 and the best-fitting models for the *XMM-Newton* and *Suzaku* data are shown in Figures 6(a) and (b), respectively. The 4–10 keV band is shown in the plots in order to exhibit details of the complex Fe K region of the spectra. The χ^2 and reduced χ^2 values in Table 3 show that the fits are essentially as good as the previous spectral fits with PEXRAV reported for the *XMM-Newton* data in Table 1 and for the *Suzaku* data in Yaqoob et al. (2007). A direct comparison of the reduced χ^2 values is given in the footnotes to Table 3. In Figure 6 the black spectra show the summed direct and reflected models and the red spectra show the reflection models only (continuum plus lines). It can be seen from both the numerical results in Table 3 and the spectra in Figure 6 that indeed the *XMM-Newton* and *Suzaku* data are consistent with the reflection spectra (continuum plus lines) following the intrinsic continuum variability. Both data sets are consistent with the same inclination angle, $\sim$40°. Further observation and more detailed self-consistent modeling of the emission line and continuum components is essential, and some of the authors of this paper have obtained observing time on NGC 2992 for an extended monitoring campaign with *XMM-Newton*, along with a quasi-simultaneous *Chandra* high-energy transmission grating observation. The new data promise to provide new insight into the properties and origins of all of the Fe Kα emission line and continuum components, and into the structures responsible for producing them.

6. DISCUSSION AND CONCLUSIONS

In the past three decades, the Seyfert galaxy NGC 2992 has shown X-ray continuum flux variations of more than a factor of 20. We have reported the results of an *XMM-Newton* observation of NGC 2992 performed in 2003, during which the source was found to have the highest 2–10 keV flux (9.4×10^{-11} erg cm^{-2} s^{-1}) compared to previous historical values. No previous X-ray astronomy mission to date has observed NGC 2992 in a high state (2–10 keV flux greater than $\sim 7 \times 10^{-11}$ erg cm^{-2} s^{-1}) with CCD spectral resolution ($\sim$7000 km s^{-1} FWHM at 6.4 keV). The best spectral resolution available for any previous high-state data set for NGC 2992 was a factor of $\sim$3 worse than that for the *XMM-Newton* data in the Fe K band. The rather unique *XMM-Newton* pn spectrum of NGC 2992 has a broad feature in the $\sim$5–7 keV band that can be interpreted as relativistic Fe Kα line emission. Its flux is an order of magnitude larger than that found in *Suzaku* data (obtained in 2005), when the 2–10 keV continuum flux of NGC 2992 was a factor of $\sim$8 less than that during the *XMM-Newton* observation. Although the detailed Fe Kα line parameters obtained from the *XMM-Newton* data are model dependent, it appears that the absolute luminosity of the broad Fe Kα line and the associated reflection continuum increase as the continuum luminosity increases.

The observation of *variable* broad, relativistic Fe Kα line emission in AGNs is rare, and the observation of such variability in response to X-ray continuum variability is even rarer. In the light-bending model (Lu & Yu 2001; Fabian & Vaughan 2003; Miniutti & Fabian 2004) invoked to account for the *non-variability* of the broad Fe Kα line in MCG −6-30-15, the X-ray continuum variability for an observer at infinity is due entirely to relativistic effects as the X-ray source physically changes position relative to the black hole. The disk, being much closer to the X-ray source and black hole than the distant observer, is then not subject to large variability in illumination by the X-ray continuum and therefore produces an Fe Kα emission line that is not variable. In this model there can of course be no intrinsic variability of the X-ray source, otherwise the Fe Kα line would be variable. The *XMM-Newton* data for NGC 2992, when considered in the context of historical data, therefore suggest that the light-bending scenario is not relevant for this AGN, implying that the large-amplitude X-ray continuum variability is *intrinsic* to the X-ray source. Further, if there were X-ray continuum variability that had *both* an intrinsic origin and one due to relative motion of the X-ray source and black hole, the broad Fe Kα line and continuum variability would not be related in a simple way.

The high level of the intrinsic continuum during the *XMM-Newton* observation reported here swamped the features that originate in circumnuclear matter that is more extended than the X-ray source because these features did not respond to the large-amplitude change in the intrinsic continuum that must have occurred prior to the start of the *XMM-Newton* observation. These features (namely the optically thin thermal emission, the scattered intrinsic continuum, and the narrow core of the Fe Kα line) have been better studied in historical spectra taken during low-continuum states (e.g., Weaver et al. 1996; Gilli et al. 2000; Yaqoob et al. 2007).

The authors thank the *XMM-Newton* instrument teams and operations staff for making the observations of NGC 2992. This research made use of the HEASARC online data archive services, supported by NASA/GSFC. The work was supported by Chinese NSF through grant 10773010/10825312 and the Knowledge Innovation Program of CAS (grant KJCX2-YW-T05).

REFERENCES

Arnaud, K. A. 1996, in ASP Conf. Ser. 101, Astronomical Data Analysis Software and Systems V, ed. G. Jacoby & J. Barnes (San Francisco, CA: ASP), 17
Bearden, J. A. 1967, Rev. Mod. Phys., 39, 78
Beckmann, V., Gehrels, N., & Tueller, J. 2007, ApJ, 666, 122
Beckwith, K., & Done, C. 2004, MNRAS, 352, 353
Brenneman, L. W., & Reynolds, C. S. 2006, ApJ, 652, 1028
Brenneman, L. W., & Reynolds, C. S. 2009, ApJ, 702, 1367
Colbert, E. J. M., Strickland, D. K., Veilleux, S., & Weaver, K. A. 2005, ApJ, 628, 113
Dadina, M. 2008, A&A, 485, 417
Dickey, J. M., & Lockman, F. J. 1990, ARA&A, 28, 215
Dovčiak, M., Karas, V., Martocchia, A., Matt, G., & Yaqoob, T. 2004a, in Proc. RAGtime 4/5 Workshops on Black Holes and Neutron Stars, ed. S. Hledìk & Z. Stuchlìk Opava (Czech Republic: Silesian Univ.), 33
Dovčiak, M., Karas, V., & Yaqoob, T. 2004b, ApJS, 153, 205
Fabian, A. C. 2006, Astron. Nachr., 327, 943
Fabian, A. C., Miniutti, G., Gallo, L., Boller, Th., Tanaka, Y., Vaughan, S., & Ross, R. R. 2004, MNRAS, 353, 1071
Fabian, A. C., Miniutti, G., Iwasawa, K., & Ross, R. R. 2005, MNRAS, 361, 795
Fabian, A. C., Rees, M. J., Stella, L., & White, N. E. 1989, MNRAS, 238, 729
Fabian, A. C., & Vaughan, S. 2003, MNRAS, 340, L28
Fabian, A. C., et al. 2002, MNRAS, 335, L1
Gilli, R., Maiolino, R., Marconi, A., Risaliti, G., Dadina, M., Weaver, K. A., & Colbert, E. J. M. 2000, A&A, 355, 485
Guainazzi, M., & Bianchi, S. 2007, MNRAS, 374, 1290
Guainazzi, M., Bianchi, S., & Dovčiak, M. 2006, Astron. Nachr., 327, 1032
Kallman, T. R., Palmeri, P., Bautista, M. A., Mendoza, C., & Krolik, J. H. 2004, ApJ, 155, 675
Lu, Y. J., & Yu, Q. J. 2001, ApJ, 561, 660
Magdziarz, P., & Zdziarski, A. A. 1995, MNRAS, 273, 837
Markowitz, A., & Edelson, R. 2004, ApJ, 617, 939
Matt, G., Guainazzi, M., & Maiolino, R. 2003, MNRAS, 342, 422
Miller, J. M. 2007, ARA&A, 45, 441
Miller, L., Turner, T. J., & Reeves, J. N. 2008, A&A, 483, 437
Miller, L., Turner, T. J., & Reeves, J. N. 2009, MNRAS, 399, 69
Miniutti, G., & Fabian, A. C. 2004, MNRAS, 349, 1435
Morse, J. A., Wilson, A. S., Elvis, M., & Weaver, K. A. 1995, ApJ, 439, 121
Murphy, K., Yaqoob, T., & Terashima, Y. 2007, ApJ, 666, 96
Nandra, K., O'Neill, P. M., George, I. M., & Reeves, J. N. 2007, MNRAS, 382, 194
Nandra, K., & Pounds, K. A. 1994, MNRAS, 268, 405
Piccinotti, G., Mushotzky, R. F., Boldt, E. A., Holt, S. S., Marshall, F. E., Serlemitsos, P. J., & Shafer, R. A. 1982, ApJ, 253, 485
Pike, C. D., et al. 1996, ApJ, 464, 487
Ponti, G., Miniutti, G., Cappi, M., Maraschi, L., Fabian, A. C., & Iwasawa, K. 2006a, MNRAS, 368, 903
Ponti, G., Miniutti, G., Fabian, A. C., Cappi, M., & Palumbo, G. G. C. 2006b, Astron. Nachr., 327, 1055
Reynolds, C. S., Young, A. J., Begelman, M. C., & Fabian, A. C. 1999, ApJ, 521, 99
Rossi, S., Homan, J., Miller, J. M., & Belloni, T. 2005, MNRAS, 360, 763
Ross, R. R., & Fabian, A. C. 2005, MNRAS, 358, 211
Turner, T. J., George, I. M., Nandra, K., & Turcan, D. 1999, ApJ, 524, 667
Turner, T. J., & Miller, L. 2009, A&AR, 17, 47
Turner, T. J., Miller, L., Kraemer, S. B., Reeves, J. N., & Pounds, K. A. 2009, ApJ, 698, 99
Turner, T. J., & Pounds, K. A. 1989, MNRAS, 240, 833
Turner, T. J., Weaver, K. A., Mushotzky, R. F., Holt, S. S., & Madejski, G. M. 1991, ApJ, 381, 85
Weaver, K. A., Nousek, J., Yaqoob, T., Mushotzky, R. F., Makino, F., & Otani, C. 1996, ApJ, 458, 160
Yaqoob, T., & Padmanabhan, U. 2004, ApJ, 604, 63
Yaqoob, T., et al. 2007, PASJ, 59, 283